Accepted Manuscript

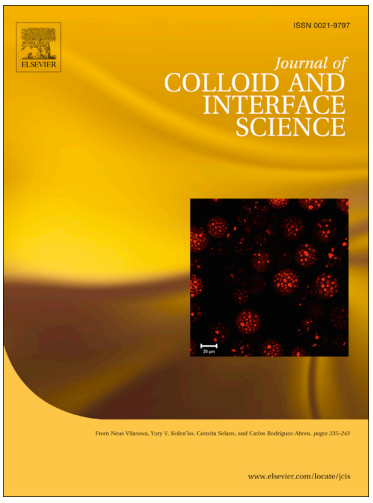

Ag modified ZnS for photocatalytic water pollutants degradation: influence of metal loading and preparation method

O. Sacco, V. Vaiano, D. Sannino, R.A. Picca, N. Cioffi

PII: S0021-9797(18)31387-0
DOI: https://doi.org/10.1016/j.jcis.2018.11.073
Reference: YJCIS 24338

To appear in: *Journal of Colloid and Interface Science*

Received Date: 5 October 2018
Revised Date: 16 November 2018
Accepted Date: 18 November 2018

Please cite this article as: O. Sacco, V. Vaiano, D. Sannino, R.A. Picca, N. Cioffi, Ag modified ZnS for photocatalytic water pollutants degradation: influence of metal loading and preparation method, *Journal of Colloid and Interface Science* (2018), doi: https://doi.org/10.1016/j.jcis.2018.11.073

Ag modified ZnS for photocatalytic water pollutants degradation: influence of metal loading and preparation method

O. Sacco[1]*, V. Vaiano[1], D. Sannino[1], R.A. Picca[2], N. Cioffi[2]

[1]University of Salerno, Department of Industrial Engineering, Via Giovanni Paolo II 132, 84084 Fisciano (SA), Italy

[2]University of Bari "Aldo Moro", Department of Chemistry, Via E. Orabona 4, 70126 Bari, Italy

* Corresponding author: Tel: + 39 089 964006; E-mail: osacco@unisa.it.

.

Abstract

In this paper, the photocatalytic degradation of organic pollutants was investigated using Ag/ZnS nanoparticles at different noble metal loadings. The photocatalysts were prepared at room temperature by two different methods: photodeposition and chemical reduction. The obtained samples were characterized by Specific surface area measurement, X-ray photoelectron spectroscopy, X-ray Powder diffraction, ultraviolet-visible diffuse reflectance and Raman spectroscopy. The X-ray photoelectron spectroscopy spectra showed that Ag is present on ZnS surface as intermediate state between nanostructured Ag^0 and Ag_2O. Moreover, the addition of silver caused a significant change of the absorption spectrum of bare ZnS, resulting in higher absorbance in the visible region, due to the Ag surface plasmon band. Methylene blue (MB) was used to evaluate the photocatalytic activity of the prepared samples. The best photocatalytic activity was observed using the sample at 0.1 wt% Ag loading prepared by chemical reduction method. In particular, the almost complete MB degradation was achieved using UV-LEDs as light sources and 6 g L^{-1} of catalyst dosage. Finally, the optimized photocatalyst was also effective in the degradation of phenol in aqueous solution under UV irradiation.

Keywords: Ag/ZnS, silver loading, UV irradiation, methylene blue, phenol

1. Introduction

Heterogeneous photocatalysis is a promising approach to protect the aquatic environment due to its ability to remove organic pollutants in water [1]. In the past two decades, many semiconducting oxides and sulfides, such as TiO_2, ZnO, WO_3, $SrTiO_3$, ZrO_2, ZnS, CdS, CuS were applied as photocatalysts for environmental control technology and also for a wide range of chemical reactions [2-6]. Among them, ZnS is an important II–VI group semiconductor existing in two main crystalline phases: α-phase (hexagonal wurtzite structure) and β-phase (cubic sphalerite structure) [7]. ZnS has been considered in different photocatalytic chemical reactions due to its relatively wide band gap value and the high negative value of the conduction band potential [8, 9]. In particular, the reported band gap energy of ZnS was 3.6 eV [10], so it can absorb light with wavelengths below 380 nm [11]. In addition, ZnS owns additional advantages, such as good thermal stability, high electronic mobility, nontoxicity, water insolubility and comparatively inexpensive cost [12].

When ZnS semiconductor is irradiated with photons of energy equal or greater than the band gap, an electron may be excited from the valence band (VB) into the conduction band (CB) leaving a hole in the VB. The electron and hole can recombine and release energy. If a suitable scavenger or surface defect is available in the semiconductor, it could trap the electron or hole and the recombination is inhibited [2]. This is a key aspect if ZnS must be used as photocatalyst. In fact, for this semiconductor, the photogenerated electrons and holes easily recombine before they take part in photocatalysis [13]. As a matter of fact, the coupling of TiO_2 and ZnO with other semiconductors or the doping with metals or non-metals is able to

suppress the electron–hole pair recombination rate and thus increasing the quantum yield [14-16].

Therefore, to retard the recombination of photoexcited electron–hole pairs and to enhance the photocatalytic efficiency of ZnS, one of the possible approaches (commonly used also for other semiconductors, such as TiO_2 [17, 18] and ZnO [19, 20]) is to couple ZnS with materials that act as electron traps and, therefore, able to extend the charge carrier lifetime [21]. Numerous investigations reported that the addition of noble metals, such as Au [22], Pt [23, 24] or Pd [25], enhances the overall photoefficiency of the semiconductors. This effect is attributed to the reduction in the recombination rate due to a better charge separation between the electrons, which accumulate on the metal, and the holes, which remain on the photocatalyst surface [26]. Compared to the other noble metals, Ag is less expensive, so Ag based photo-catalysts may receive greater attention for industrial practice [27-29].

Many papers describe the effects of doping ZnS with silver [30-32]. In contrast, only few studies report the effects of Ag deposited on ZnS nanoparticles [21]. However, from our knowledge of the pertinent literature, no paper concerning the influence of Ag content on a ZnS surface for photocatalytic applications has been published.

Therefore, this paper reports the enhanced photocatalytic removal of organic pollutants using Ag/ZnS nanoparticles at different noble metal loadings. The photocatalysts were prepared using two different techniques (photodeposition and chemical reduction). The influence of the noble metal loading on ZnS surface and the preparation method was evaluated in terms of the photodegradation of methylene blue (MB) as model organic cationic dye. Furthermore, the effect of various operating parameters, such as dye concentration, photocatalyst dosage as well as

light sources was studied on the best sample. Finally, the optimized Ag/ZnS photocatalyst was tested in the removal of phenol.

2. Materials and methods

2.1 Materials

Zinc sulfide (ZnS), sodium borohydride ($NaBH_4$) and silver nitrate ($AgNO_3$) were purchased from Sigma–Aldrich. The model water pollutants (methylene blue and phenol) were purchased from Sigma–Aldrich.

2.2 Synthesis of the Ag/ZnS nanoparticles using the chemical reduction method

The Ag/ZnS photocatalysts were synthesized through chemical reduction method starting from 1 g of the commercial ZnS suspended into 100 mL of distilled water containing different amounts of $AgNO_3$ (in the range 0.785-3.1 mg). The prepared reaction mixture was then stirred and a gaseous helium flow (flow rate: 30 $NL \cdot h^{-1}$) was bubbled inside the suspension.

Afterward, the reducing agent ($NaBH_4$) was added into the system. The added quantity of $NaBH_4$ was calculated with respect to the amount of $AgNO_3$ considering the stoichiometric ratio of the following reaction with an excess equal to 30%:

$$2\ AgNO_3 + 2\ NaBH_4 = 2\ Ag + H_2 + 2\ NaNO_3 + B_2H_6 \qquad \text{Eq.1}$$

The suspension was left under stirring in presence of the helium flow for 1 h, washed with distilled water for three times and finally dried overnight at room temperature.

The obtained Ag/ZnS photocatalysts are denoted as xAg, where x indicates the nominal Ag loading expressed as weight percentage (wt %) (Eq. 2).

$$\%Ag = \frac{gAg}{gAg + gZnS}\ 100 \qquad \text{Eq.2}$$

Where:

gAg is the weight of silver calculated from the amount of $AgNO_3$ used in the preparation;

gZnS is the weight of the commercial ZnS used in the preparation.

2.3 Synthesis of the Ag/ZnS nanoparticles using the photodeposition method

The Ag/ZnS photocatalysts were synthesized through photodeposition method starting from 1 g of the commercial ZnS suspended into 100 mL of distilled water at room temperature containing 1.55 mg of $AgNO_3$. Then, the reaction system was irradiated for 1h by two UV lamps emitting at 365 nm (nominal power: 8 W each, provided by Philips). Helium (flow rate: 30 $NL \cdot h^{-1}$) was bubbled inside the suspension during the overall irradiation time.

The photochemical reactions occurring during the photodeposition are summarized as follows [24]:

$$ZnS + h\nu \rightarrow e^-(CB) + h^+(VB) \qquad \text{Eq.3}$$

$$Ag^+ + e^-(CB) \rightarrow Ag^0 \qquad \text{Eq.4}$$

$$2H_2O + h^+(VB) \rightarrow O_2 + 4H^+ \qquad \text{Eq.5}$$

After the photodeposition, the suspension was centrifuged, washed with distilled water for three times and finally dried overnight at room temperature.

All the prepared samples are listed in Table 1.

Table 1

2.4 Characterization of the Ag/ZnS photocatalysts

Different characterization techniques were used to analyze the Ag/ZnS photocatalysts. In particular, the specific surface area (SSA) measurement was performed by BET method using N_2 adsorption at -196 °C with a Costech Sorptometer 1042 after a pretreatment at 35°C for 2 hours in He flow (99.9990 %). X-ray photoelectron spectroscopy (XPS) characterization was performed on a PHI Versaprobe II spectrometer using monochromatized Al Kα radiation (1486.6 eV). Both survey and high-resolution (HR) spectra were acquired. Pass energy of 117.4 eV and an energy step of 1.0 eV were used in the former case, whereas a pass energy of 58.7 eV and an energy step of 0.125 eV in the latter. C1s, O1s, Ag3d, S2p, N1s, $Zn2p_{3/2}$, $ZnL_3M_{45}M_{45}$ regions were analyzed. Surface elemental composition was evaluated by MultiPack™ (v. 9.5.0, PHI-ULVAC) software. Peak fitting was carried out on CasaXPS™ (v. 2.3.18). Binding energy (BE) scale was corrected taking as reference the C1s aliphatic component at 284.8 eV.

The crystalline phases of the Ag/ZnS samples were determined by X-ray Powder diffraction (XRD) patterns, obtained by using a Brucker D8 diffractometer with CuKα (λ = 0.154 nm) radiation. The diameter of the crystalline grain was calculated according to Scherrer's formula [33].

The ultraviolet-visible diffuse reflectance spectra (UV-vis DRS) of the Ag/ZnS samples were recorded using a Perkin Elmer spectrometer Lambda 35 by means of a RSA-PE-20 reflectance spectroscopy accessory (Labsphere Inc., North Sutton, NH). The optical band gap (E_{bg}) values of the photocatalysts were determined through the corresponding Kubelka–Munk function (KM) (which is proportional to the absorption of radiation) and by plotting $(KM \times h\upsilon)^2$ against $h\upsilon$. The Raman spectra

were recorded using a Dispersive MicroRaman spectrometer (Invia, Renishaw) with a laser emitting at 514 nm.

2.5 Photocatalytic tests

Methylene blue (MB) solutions were prepared by dissolving 15 mg in 1L of MilliQ-grade water to obtain an initial dye concentration equal to 15 mg L^{-1}. Phenol solutions were prepared by dissolving 25 mg in 1L of MilliQ-grade water to obtain an initial phenol concentration equal to 25 mg L^{-1}.

The experiments were realized using a pyrex cylindrical photoreactor (ID= 2.5 cm) equipped with an air distributor device (Q_{air}=9 NL·h^{-1}), a magnetic stirrer to maintain the photocatalyst suspended in the aqueous solution and a temperature controller. Four UV lamps (nominal power: 8 W each, provided by Philips) or UV-LEDs (nominal power: 12 W, provided by LEDlightinghut) strips, emitting at 365 nm, were used as light sources.

The UV lamps were placed around the external surface of the photoreactor at an equal distance from it (about 30 mm), while, the LEDs strip was positioned around and in contact with the external body of the photoreactor. Prior to the irradiation, the suspension was left in dark conditions for 120 min to reach the dye adsorption/desorption equilibrium on the photocatalyst surface and after, the photocatalytic test was begun under the UV light irradiation up to 180 min.

During the irradiation time, slurry samples (about 2 mL) were withdrawn at fixed time and then they were centrifuged to remove the catalyst powders before the concentration measurement by a Perkin Elmer UV-Vis spectrophotometer at 663 nm for MB concentration [34] and at 270 nm for phenol concentration [35].

3. Results and Discussion

3.1 Characterization of the photocatalysts

3.1.1 Specific surface area (SSA)

The SSA values of all the samples are reported in Table 1. In particular, for the Ag/ZnS samples prepared by the chemical reduction method, the SSA values did not change significantly with respect to the commercial ZnS (17 $m^2 \cdot g^{-1}$) when the Ag content was in the range 0.05-0.1 wt%. With the increase of the Ag content up to 4 wt%, the SSA decreased to 13 $m^2 \cdot g^{-1}$, due to a possible agglomeration of the Ag nanoparticles on the ZnS surface, as previously observed in literature for the Ag deposited on semiconductor surface [36]. A similar SSA value was achieved for the 0.1Ag and 0.1Ag(F) samples, indicating that the preparation method did not influence the textural characteristics of the final samples.

3.1.2 X-ray photoelectron spectroscopy (XPS)

XPS characterization was carried out on the pristine ZnS powder and on the different Ag/ZnS samples, evaluating the surface loading of the metal as well as the element chemical speciation. Zn, S, and Ag (only in doped specimens) as well as C and O were detected. The presence of the last two elements was expected, considering that the samples were stored in air, and no sputtering treatment (e.g. with Ar^+) was performed before acquiring XP spectra. The typical surface composition of all the analyzed materials is reported in Table 2.

Table 2

The stoichiometric ratio for ZnS is preserved in all the cases. The silver surface

availability tends to increase with the nominal Ag wt%, although the Ag content is similar for 0.1Ag, 0.1(F)Ag, and 0.5Ag samples. This suggests that there is not a dramatic influence of the synthesis process on the silver surface content, in agreement with other characterizations carried out in this work. Interestingly, the surface Ag content determined by XPS is by far higher than the nominal one. This is reasonable, since the nominal Ag wt% is relevant to the bulk composition, while the data calculated from the XPS analyses are related to the outer nanomaterial surface. In other words, the silver is more present at the outer layers. Additionally, the successful reduction of the silver nitrate precursor and the removal of unreacted precursor (if any) upon sample washing were proven since no nitrogen XP signal was detected, even on the 4Ag catalyst. S2p and ZnLMM signals are reported for both the commercial ZnS and 0.1Ag samples in Figure 1. $S2p_{3/2}$ falls at BE = 161.6 ± 0.1 eV, characteristic of ZnS [37]. ZnLMM position at kinetic energy (KE) equal to 989.4 ± 0.2 eV is also compatible with ZnS [37].

Figure 1

It can be observed that there is no effect on the ZnS matrix (in terms of peak shift and/or lineshape modification) associated to the Ag presence; this holds true also at the highest Ag loading (data not shown). The silver speciation was studied by investigating both Ag3d and $AgM_{45}N_{45}N_{45}$ Auger signals [38]. Typical Ag3d region is presented in Figure 2a for the 0.1Ag sample; the same region showing no peak was also reported for pristine ZnS for comparison. A single doublet can be observed for 0.1Ag, whose $Ag3d_{5/2}$ component is centered at BE = 368.2 ± 0.1 eV. Peak position was unchanged at the other Ag loadings. Unfortunately, the chemical shift on Ag3d

position associated to different silver chemical environments is generally small, and their discrimination is better achieved if AgMNN region is considered [38, 39]. This signal has a lower intensity and was detectable only for nominal Ag wt% ≥ 2. When measurable, the AgMNN spectra indicated that Ag is essentially present as slightly oxidized nanoparticles [37]. AgMNN spectrum acquired on the 4Ag sample is shown in Figure2b. The most informative position (indicated by the dotted line) falls at KE = 356.8 ± 0.2 eV, which is attributed to an intermediate state between nanostructured Ag^0 and Ag_2O. Such finding can be easily explained in terms of formation of uncapped silver nanoclusters, which undergo partial oxidation upon air exposure [38].

Figure 2

3.1.3 X-ray diffraction (XRD)

The XRD patterns of the commercial ZnS together with the prepared Ag/ZnS photocatalysts were recorded and the results are shown in Figure 3.

Figure 3

The patterns of all the samples showed a peak at about 2θ = 28.4°, which can be indexed as the (110) reflection of α-phase of ZnS (wurtzite) [40] and at 28.37°, 33.19°, 47.63°, 56.49° and 76.95°, indexed respectively as (111), (200), (220), (311) and (331), all assigned to β-phase of ZnS (cubic blende) [41, 42]. Since the (002) and (110) planes of the ZnS wurtzite structure overlap with the (111) and (022) planes of the ZnS β-phase, the structures of both the commercial ZnS and the

Ag/ZnS samples can be regarded as a mixture of ZnS α-phase and β-phase with a dominant cubic sphalerite structure (β-phase).

No peak for Ag is detectable for any of the Ag/ZnS samples. This is probably an indication of a better dispersion and smaller metal particle size for Ag (which make it undetectable with XRD technique), or to an incomplete reduction of the Ag [43, 44]. Finally, no difference in the XRD patterns of the 0.1Ag and 0.1Ag(F) samples is observed (Figure 3b).

Furthermore, the ZnS crystallite size of the samples was calculated using the Sherrer's formula based on the XRD patterns and considering the diffraction peak at 2θ~28.4° (Table 1). According to these calculations, the average crystallite size of the commercial ZnS and Ag/ZnS samples was approximately constant up to 0.1 wt% Ag content and it was equal to 23 nm. In addition, it is important to underline that the preparation method did not induce differences in crystallite size of the samples. On the contrary, by increasing the Ag amount up to 4 wt%, it is possible to observe also an increase of crystallite size up to 26 nm. A similar behavior has been reported for Ag/ZnO and Ag/TiO_2 photocatalysts [44, 45].

3.1.4 UV-Vis reflectance spectroscopy (UV-vis DRS)

The Kubelka-Munk curves, derived from the reflectance spectra of the photocatalysts, are shown in Figure 4.

Figure 4

The commercial ZnS sample did not absorb light in the visible region and evidenced an absorption onset at about 360 nm with maximum absorbance at 330 nm.

Compared to the commercial ZnS, the Ag/ZnS samples exhibited an increase of absorption in the UV region up to 2 wt% Ag content. In detail, the intensity of the main band in the range 200-360 nm increased together with the increase of Ag loading from 0.05 to 0.1 wt% and progressively decreased for the 0.5Ag and 2Ag samples, until the complete disappearance for 4Ag sample. The obtained trend is in agreement with the UV-vis DRS analysis performed on Ag-TiO_2 photocatalysts [45]. For 0.05Ag, 0.1Ag, 0.5Ag and 2Ag samples, beyond the absorption threshold of ZnS at $\lambda \leq 360$ nm, it was observed that the addition of silver caused a significant change of the absorption spectrum of bare ZnS, resulting in high absorbance from 400 nm to the entire visible region, due to the Ag surface plasmon band [46, 47]. In particular, the higher the amount of Ag content, the greater was the absorption in the visible region [21, 44]. This absorption is due to the presence of the Ag nanoparticles, coherently with the observation made by Yang et al. [48] regarding semiconducting materials modified with silver. A completely different absorption spectrum was achieved for 4Ag sample, evidencing only a main broad band centered at about 440 nm, due to Ag nanoparticles [49] that, probably, cover the entire ZnS surface.

The absorptions below 400 nm should be attributed to the formation of silver clusters partially or totally reduced, whose stoichiometry can range from Ag_2^+ to $Ag_n^{\delta+}$. In particular, a maximum in the absorbance at 337 nm, with shoulders at around 320 and 275 nm, is observed for the 0.1Ag sample. These absorptions indicate that the charged clusters have different nuclearity. In particular, Ag_2^+ and Ag_4^{2+} are retained to give bands at 340 and 270 nm, respectively [50]. The bands at 320 and 285 nm were typical for the absorption of neutral Ag_8 and charged Ag_8^+ clusters, respectively [51].

However, from the comparison between the spectra of the 0.1Ag and 0.1Ag(F)

samples (Figure 4b), the different intensity of the absorption in the range 200-400 nm may indicate a higher reduction degree of silver clusters with the photoreduction method, since the absorption at around 320 nm (to be attributed to the neutral Ag_8 clusters) increases [52].

The E_{bg} values of the samples are reported in Table 1. The E_{bg} of the commercial ZnS is equal to 3.5 eV. The increase of Ag loading from 0.05 up to 0.5 wt% resulted in a slight decrease of the E_{bg} that was equal to 3.4 eV for all the samples. The further increase in Ag loading (2Ag and 4Ag samples) caused a reduction of the calculated E_{bg}, being equal to 2.1 and 1.8 eV, respectively. The observed strong decrease of E_{bg} for 2Ag and 4Ag may be due to the high concentration of Ag nanoparticles on ZnS surface [53]. This drastic decrease in E_{bg} can also explain the changes in UV-visible absorption properties and clearly indicates a progressive metallization of the samples caused by the Ag [53].

These observations suggest that the amount of the Ag loaded on ZnS has an important effect on E_{bg}. The Mulliken electronegativity theory [54] was used for empirically determining the valence band (VB) edge potential (E_{VB}) of a ground-state semiconductor by using the following equation:

$$E_{VB} = X_{Semiconductor} - E_e + 0.5E_{bg} \qquad \text{Eq.6}$$

Where:

$X_{Semiconductor}$ is the electronegativity of the semiconductor (in this case 5.26 eV)[55];

E_e is the energy of free electrons on the hydrogen scale (ca. 4.5 eV);

E_{bg} is the optical band gap energy of the semiconductor (calculated by the method described above).

The CB edge potential (E_{CB}) can be determined using the following relationship [56]:

$$E_{CB} = E_{VB} - E_{bg} \quad \text{Eq.7}$$

Because the E_{bg} of the commercial ZnS is 3.5 eV (Table 1), the estimated E_{VB} is 2.51 eV, and the corresponding E_{CB} is −0.99 eV. In contrast, the presence of Ag up to 0.5 wt% loading determined a little variation of the E_{VB} and E_{CB} values (Table 1) meaning that the Ag/ZnS samples can maintain the strong redox potentials [57]. Ag species loaded on the surface of ZnS can effectively capture the photoinduced electrons and holes. In addition, the photoinduced electrons can quickly be transported to the species adsorbed on the surface of ZnS under UV irradiation [58]. From the comparison between 0.1Ag and 0.1Ag(F) samples, it was evidenced that, at the same Ag nominal loading and using the two different preparation methods, no difference in terms of E_{bg} and consequently no dissimilarity in terms of E_{VB} and E_{CB} values were observed.

For the 2Ag and 4Ag samples, the E_{bg} value was lower than the other samples and in particular it was equal to 2.1 and 1.8 eV for 2Ag and 4Ag, respectively.

3.1.5 Raman spectroscopy

The Raman spectra of the samples are shown in Figure 5.

Figure 5

It is possible to observe that the commercial ZnS exhibited a main peak at 352 cm^{-1}, commonly referred to LO mode [59, 60] of cubic blende zinc sulfide. In addition to

this LO peak, several weaker peaks are identified as pure acoustic or optical modes and combinations of these [59-61].

After the addition of silver (Figure 5a), the intensity of the bands located at about 260 and 352 cm^{-1}, associated to ZnS, decreased and become broader up to 0.5 wt% Ag loading. This phenomenon was due to the modifications in the ZnS interatomic distances with a surface pressure increase induced by the increase of the Ag content in Ag/ZnS samples [62]. For 2 and 4wt % Ag loading, the main bands of the bare ZnS tend to disappear, as previously observed for Ag/TiO_2 [62].

Furthermore, the Ag deposition on the ZnS surface was confirmed by the detection of additional Raman bands. In particular, the signal at about 215 cm^{-1} (whose intensity increased up to 0.5 wt% Ag content) could be associated to the radial effect of Ag atoms [63]. For 2Ag and 4Ag photocatalysts, the broad Raman bands in the range 380-580 cm^{-1} are due to the presence of silver atoms producing polar branches of A_1(TO) and A_1(LO) fundamental modes of Raman scattering [64]. Finally, the comparison between the Raman spectra of 0.1Ag and 0.1Ag(F) evidenced that, at the same Ag nominal loading, the sample prepared by the chemical reduction method showed the band located at 215 cm^{-1} with higher intensity than that one observed for the sample prepared through the photodeposition method (Figure 5b).

3.2 Photocatalytic Activity

3.2.1 Photocatalytic decolourization of MB: influence of the Ag loading on ZnS

The photocatalytic degradation of MB under UV light irradiation was investigated using the commercial ZnS and Ag/ZnS photocatalysts. The photocatalytic degradation was carried out using 100 mL of MB solution with an initial dye concentration of 15 mg L^{-1} and a catalyst dosage of 3 $g \cdot L^{-1}$.

Figure 6

The obtained results are reported in Figure 6. For all the Ag/ZnS samples, it is possible to observe that the presence of Ag increased the MB adsorption in dark conditions with respect to the commercial ZnS. In detail, the MB relative concentration decreased from 7 to about 14% for 0.05Ag and 0.1Ag, respectively. On the other hand, for Ag loading higher than 0.1 wt% (0.5Ag, 2Ag and 4Ag samples), the decrease of MB concentration was lower and about 11%.

After the dark period, the solution was irradiated by UV lamps and the reaction started to occur. Under irradiation, the MB relative concentration progressively decreased for ZnS, 0.05Ag, 0.1Ag and 0.5Ag. In particular, using the commercial ZnS, the MB decolourization degree was equal to 45% after 180 min of UV irradiation.

It is worthwhile to note that, at the same irradiation time (180 min), the MB decolourization increased with the increase of Ag content up to 0.1wt %, while for higher metal loading (0.5wt %) the photocatalytic activity of the samples decreased until to be totally inhibited for 2Ag and 4Ag samples. The 0.1Ag photocatalyst demonstrated the highest activity among all the tested catalysts, leading to an MB decolourization equal to 55% in 180 min, thus indicating that the optimal Ag content was equal to 0.1wt %. This last result could be attributed to the presence of Ag on the ZnS surface that effectively inhibits the recombination of photoinduced electron and hole pairs [65]. This observation is consistent with the UV-vis DRS spectra (Figure 4) since it was evidenced the presence of Ag plasmon band. Possibly, a large

number of photoexcited electrons were generated from the Ag particles surfaces to the conduction band of the ZnS and consequently the photocatalytic activity increased [66].

On the other hand, the decrease of photocatalytic activity, observed at higher Ag content (0.5Ag), can be explained considering that Ag particles may act as a recombination center due to the increase of Ag particle size on ZnS surface (as argued from the reduction of specific surface area) [67]. This effect probably determined the worsening of the photocatalytic activity, as also observed in the literature [68]. The total inhibition of photocatalytic activity, observed for 2Ag and 4Ag, could also be explained considering the very low optical band-gap value of these samples (2.1 eV for 2Ag and 1.8 eV for 4Ag), which brings to the inhibition of MB photodegradation process because of the possible more facile electron/hole recombination in the excited state of the catalyst [21].

3.2.2 Photocatalytic decolourization of MB: comparison between UV lamps and UV-LEDs

Figure 7 shows the comparison of the photocatalytic experiments carried out using two different external light sources (UV lamps or UV-LEDs), at the same initial MB initial concentration (15 mgL^{-1}) and 0.1Ag catalyst dosage (3g L^{-1}).

Figure 7

The obtained results showed that, after 180 min of UV exposure time, in the case of UV lamps, the MB decolourization was equal to 55% while, when UV-LEDs are

used as light sources, the MB decolourization increased up to 76%. This last result can be explained considering that the use of the UV-LEDs strip allows to reduce the dispersion of the UV photons in the external environment thanks to its geometry [69] and the higher luminous efficiency for the LEDs that allows to increase the number of photons per hour entering into the reactor [69, 70].

3.2.3 Photocatalytic decolourization of MB: comparison between the different synthesis methods (0.1Ag and 0.1Ag(F))

In order to compare the efficiency of the Ag/ZnS samples prepared by different synthesis method (chemical reduction and photodeposition), additional photocatalytic tests were carried out on 0.1Ag and 0.1Ag(F) samples, at the same initial MB initial concentration (15 mgL^{-1}) and catalyst dosage (3g L^{-1}).

Figure 8

After 180 min of irradiation time, the MB decolourization for 0.1Ag (76%) was noticeably higher than 0.1Ag(F) (54%). Since no significant differences were observed from XPS results, it is most probable that the decrease of absorption in the UV region (Figure 4) for the sample 0.1Ag(F) (associated to the formation of Ag~ cluster) may be responsible for the lower photocatalytic activity [71].

3.2.4 Photocatalytic decolourization of MB: influence of initial dye concentration

The effect of MB initial concentration (in the range 2.5-15 $mg \cdot L^{-1}$) has been investigated by using 0.1Ag catalyst (Figure 9).

Figure 9

The adsorption in dark conditions evidenced that the amount of MB adsorbed on the 0.1Ag surface was almost constant and equal to 6.6±1.5mg/g_{cat} for all the tested MB initial concentrations. Under UV irradiation, at the lowest investigated dye concentration (2.5 mg L^{-1}), the MB decolourization was almost complete while it was lower when MB initial concentration increased up to 15 mg L^{-1}. This behavior can be explained on the basis of change in optical absorption of the MB solutions at different dye concentration [72]. In particular, the colour of solutions increased with the increase in the MB concentration, limiting the penetration of the light in the aqueous medium [73] and, consequently, the photocatalytic activity was lower.

3.2.5 Photocatalytic decolourization of MB: influences of the 0.1Ag dosage

The effect of the 0.1Ag photocatalyst dosage (in the range 1.5-7.5 g·L^{-1}) has been investigated at 15 mg L^{-1} MB initial concentration.

Figure 10

Figure 10 shows that the photocatalytic activity increased with the increase of the 0.1Ag dosage from 1.5 to 6 g·L^{-1}, reaching the almost complete MB decolourization after 180 min of UV irradiation time. The observed enhancement is probably due to an increased number of available adsorption and catalytic sites on the surface of

0.1Ag photocatalyst [74]. When the dosage of 0.1Ag was increased up to 7.5 g L^{-1}, the decolourization rate did not change significantly. These results, commonly observed for the photocatalytic slurry systems [74], can be explained considering that when the photocatalyst dosage in the aqueous medium is too high, the solution becomes turbid and the UV light was not able to penetrate and interact with the photocatalyst [75]. Moreover, a possible additional explanation of the previous result is that the high amount of catalyst may generate particles aggregation phenomena [34] that induces the scattering of UV light, leading to the worsen of the photodegradation efficiency.

3.2.6 Photocatalytic degradation of phenol

In order to evaluate the efficiency of the 0.1Ag photocatalyst with a colorless pollutant, a photocatalytic test has been carried out using an aqueous solution containing phenol. In particular, the photocatalytic degradation of phenol under UV light irradiation using the commercial ZnS and 0.1Ag photocatalyst was investigated Figure 11.

Figure 11

For both samples, in dark conditions, the adsorption equilibrium reached the same value indicating that the presence of Ag did not affect the phenol adsorption. A different trend was observed under UV light. In fact, using the 0.1Ag photocatalyst, after 180 min of UV irradiation, the degradation of phenol was equal to 60% while the presence of only commercial ZnS led to a phenol degradation of only 27%.

4. Conclusions

In summary, in this work, the influence of Ag content on ZnS semiconductor for the photocatalytic degradation of methylene blue under UV light irradiation was investigated for the first time. It was observed an enhancement of photocatalytic activity induced by the silver addition in comparison to the bare ZnS up to 0.1 wt% Ag content. This enhancement is attributed to the presence of the silver plasmon band, which is able to generate a larger number of photoexcited electrons from the Ag particles surface to the conduction band of ZnS. Moreover, photocatalytic results evidenced that the Ag/ZnS sample prepared by chemical reduction method showed higher performances with respect to the sample prepared with photodeposition method. Finally, the optimized Ag/ZnS photocatalyst was also able to effectively degrade phenol in aqueous solution under UV irradiation. The current work may open new ways for the improvement of the photocatalytic performances of ZnS based nanoparticles for water and wastewater treatment.

References

[1] S. Ameen, M.S. Akhtar, Y.S. Kim, O.-B. Yang, H.-S. Shin, Colloid and Polymer Science 288 (2010) 1633.
[2] M.R. Hoffmann, S.T. Martin, W. Choi, D.W. Bahnemann, Chemical Reviews 95 (1995) 69.
[3] J. Soria, J. Sanz, M.J. Torralvo, I. Sobrados, C. Garlisi, G. Palmisano, S. Çetinkaya, S. Yurdakal, V. Augugliaro, Applied Catalysis B: Environmental 210 (2017) 306.
[4] M. Bellardita, V. Loddo, G. Palmisano, I. Pibiri, L. Palmisano, V. Augugliaro, Applied Catalysis B: Environmental 144 (2014) 607.
[5] C. Liu, Z. Liu, Y. Li, Z. Liu, Y. Wang, L. E, J. Ya, N. Gargiulo, D. Caputo, Materials Science and Engineering: B 177 (2012) 570.
[6] L. Li, J. Ya, L. Xiang, Z. Liu, E. Lei, Applied Physics A 123 (2017) 667.
[7] X. Fang, T. Zhai, U.K. Gautam, L. Li, L. Wu, Y. Bando, D. Golberg, Progress in Materials Science 56 (2011) 175.

[8] J. Zhang, Y. Wang, J. Zhang, Z. Lin, F. Huang, J. Yu, ACS Applied Materials & Interfaces 5 (2013) 1031.
[9] V. Vaiano, O. Sacco, D. Sannino, P. Ciambelli, Journal of Cleaner Production 100 (2015) 208.
[10] J.N. Hart, M. Cutini, N.L. Allan, Energy Procedia 60 (2014) 32.
[11] M. Mehrabian, Z. Esteki, Optik - International Journal for Light and Electron Optics 130 (2017) 1168.
[12] S.K. Maji, A.K. Dutta, D.N. Srivastava, P. Paul, A. Mondal, B. Adhikary, Polyhedron 30 (2011) 2493.
[13] M. Jakob, H. Levanon, P.V. Kamat, Nano Letters 3 (2003) 353.
[14] J.C. Colmenares, R. Luque, J.M. Campelo, F. Colmenares, Z. Karpiński, A.A. Romero, Materials 2 (2009) 2228.
[15] O. Ola, M.M. Maroto-Valer, Applied Catalysis A: General 502 (2015) 114.
[16] A.B. Lavand, Y.S. Malghe, Journal of King Saud University - Science 30 (2018) 65.
[17] E. Albiter, M.A. Valenzuela, S. Alfaro, G. Valverde-Aguilar, F.M. Martínez-Pallares, Journal of Saudi Chemical Society 19 (2015) 563.
[18] M. Antoniadou, V.M. Daskalaki, N. Balis, D.I. Kondarides, C. Kordulis, P. Lianos, Applied Catalysis B: Environmental 107 (2011) 188.
[19] M.-K. Lee, G. Tae, W. Kim, T. Kim, Y.-M. Sung, Surface Plasmon Resonance (SPR) Electron and Energy Transfer in Noble Metal− Zinc Oxide Composite Nanocrystals 112 (2008) 10079.
[20] K.S. Ranjith, R.B. Castillo, M. Sillanpaa, R.T. Rajendra Kumar, Applied Catalysis B: Environmental 237 (2018) 128.
[21] M. Madkour, F. Al-Sagheer, Optical Materials Express 27 (2016) 158.
[22] A. Bumajdad, M. Madkour, Y. Abdel-Moneam, M. El-Kemary, Journal of Materials Science 49 (2014) 1743.
[23] K. Saeed, I. Khan, T. Gul, M. Sadiq, Applied Water Science 7 (2017) 3841.
[24] V. Vaiano, M. Matarangolo, J.J. Murcia, H. Rojas, J.A. Navío, M.C. Hidalgo, Applied Catalysis B: Environmental 225 (2018) 197.
[25] R.M. Mohamed, E.S. Baeissa, Applied Catalysis A: General 464-465 (2013) 218.
[26] S. Sato, J.M. White, Chemical Physics Letters 72 (1980) 83.
[27] Y.-C. Liang, C.-C. Wang, C.-C. Kei, Y.-C. Hsueh, W.-H. Cho, T.-P. Perng, The Journal of Physical Chemistry C 115 (2011) 9498.
[28] F. Sun, X. Qiao, F. Tan, W. Wang, X. Qiu, Journal of Materials Science 47 (2012) 7262.
[29] H. Mou, C. Song, Y. Zhou, B. Zhang, D. Wang, Applied Catalysis B: Environmental 221 (2018) 565.
[30] A. Sud, R.K. Sharma, Journal of Engineering Science Invention Research & Development 3 (2016) 198.
[31] E. Hao, Y. Sun, B. Yang, X. Zhang, J. Liu, J. Shen, Journal of Colloid and Interface Science 204 (1998) 369.
[32] V.K. Gupta, A. Fakhri, M. Azad, S. Agarwal, Journal of Colloid and Interface Science 510 (2018) 95.
[33] B.E. Warren, X-ray Diffraction. Dover Publications, 1990.
[34] V. Vaiano, O. Sacco, D. Sannino, W. Navarra, C. Daniel, V. Venditto, Journal of Photochemistry and Photobiology A: Chemistry 336 (2017) 191.
[35] C.-H. Chiou, R.-S. Juang, Journal of Hazardous Materials 149 (2007) 1.
[36] H. Wang, X. Liu, S. Han, CrystEngComm 18 (2016) 1933.

[37] N.I.o.S.a. Technology, in: (Ed.)^(Eds.), Gaithersburg MD, 20899, (2012).
[38] R.A. Picca, F. Paladini, M.C. Sportelli, M. Pollini, L.C. Giannossa, C. Di Franco, A. Panico, A. Mangone, A. Valentini, N. Cioffi, ACS Biomaterials Science & Engineering 3 (2017) 1417.
[39] R.A. Picca, C.D. Calvano, M.J. Lo Faro, B. Fazio, S. Trusso, P.M. Ossi, F. Neri, C. D'Andrea, A. Irrera, N. Cioffi, Journal of Mass Spectrometry 51 (2016) 849.
[40] G. Wang, B. Huang, Z. Li, Z. Lou, Z. Wang, Y. Dai, M.-H. Whangbo, Scientific Reports 5 (2015) 8544.
[41] J.F. Xu, W. Ji, J.Y. Lin, S.H. Tang, Y.W. Du, Appl. Phys. A: Mater. Sci. Process. 66 (1998) 639.
[42] M. Bodke, U. Gawai, H. Khawal, B. Dole, Bionano frontier. 8 (2015) 131.
[43] J. Matos, B. Llano, R. Montaña, P.S. Poon, M.C. Hidalgo, Environmental Science and Pollution Research 25 (2018) 18894.
[44] C. Jaramillo-Páez, J.A. Navío, M.C. Hidalgo, Journal of Photochemistry and Photobiology A: Chemistry 356 (2018) 112.
[45] S.I. Mogal, V.G. Gandhi, M. Mishra, S. Tripathi, T. Shripathi, P.A. Joshi, D.O. Shah, Industrial & Engineering Chemistry Research 53 (2014) 5749.
[46] P. Christopher, H. Xin, S. Linic, Nature Chemistry 3 (2011) 467.
[47] Z. Xuming, C. Yu Lim, L. Ru-Shi, T. Din Ping, Reports on Progress in Physics 76 (2013) 046401.
[48] D. Yang, Y. Sun, Z. Tong, Y. Tian, Y. Li, Z. Jiang, The Journal of Physical Chemistry C 119 (2015) 5827.
[49] L. Gharibshahi, E. Saion, E. Gharibshahi, A.H. Shaari, K.A. Matori, E. Gharibshahi, Materials (Basel) 10 (2017) doi:10.3390/ma10040402.
[50] A.N. Pestryakov, A.A. Davydov, Journal of Electron Spectroscopy and Related Phenomena 74 (1995) 195.
[51] I. Tuzovskaya, N. Bogdanchikova, A. Pestryakov, V. Gurin, A. Simakov, V. Lunin, Comparison of gold and silver species supported and incorporated into mordenites. 2003.
[52] Y. Kotolevich, E. Kolobova, E. Khramov, J.E. Cabrera Ortega, M.H. Farías, Y. Zubavichus, R. Zanella, J.D. Mota-Morales, A. Pestryakov, N. Bogdanchikova, V.C. Corberán, Molecules 21(4) (2016) 532.
[53] P. Barone, F. Stranges, M. Barberio, D. Renzelli, A. Bonanno, F. Xu, 2014 (2014) http://dx.doi.org/10.1155/2014/589707.
[54] R.S. Mulliken, The Journal of Chemical Physics 2 (1934) 782.
[55] L.R. Hou, C.Z. Yuan, Y. Peng, Journal of Molecular Catalysis A: Chemical 252 (2006) 132.
[56] C. Xu, Y. Liu, B. Huang, H. Li, X. Qin, X. Zhang, Y. Dai, Applied Surface Science 257 (2011) 8732.
[57] L. Yuan, B. Weng, J.C. Colmenares, Y. Sun, Y.-J. Xu, Small 13 (2017) 1702253.
[58] Y. Zhou, G. Chen, Y. Yu, Y. Feng, Y. Zheng, F. He, Z. Han, Physical Chemistry Chemical Physics 17 (2015) 1870.
[59] S. Kim, T. Kim, M. Kang, S.K. Kwak, T.W. Yoo, L.S. Park, I. Yang, S. Hwang, J.E. Lee, S.K. Kim, S.-W. Kim, Journal of the American Chemical Society 134 (2012) 3804.
[60] A.V. Baranov, Y.P. Rakovich, J.F. Donegan, T.S. Perova, R.A. Moore, D.V. Talapin, A.L. Rogach, Y. Masumoto, I. Nabiev, Physical Review B 68 (2003) 165306.

[61] H Linfeng, M. Chen, W. Shan, T. Zhan, M. Liao, X. Fang, X. Hu, L. Wu, Advanced Materials 24 (2012) 5872.
[62] Z.V. Quinones-Jurado, M.A. Waldo-Mendoza, H.M. Aguilera-Bandin, E.G. Villabona-Leal, E. Cervantes-Gonzalez, E. Perez, Materials Sciences and Applications 5 (2014) 895.
[63] M. Buşilă, V. Musat, T. Textor, V. Badilita, B. Mahltig, Journal of Alloys and Compounds, 610 (2014) 244.
[64] S. Adhikari, A. Banerjee, N.K. Eswar, D. Sarkar, G. Madras, RSC Advances 5 (2015) 51067.
[65] J. Liqiang, W. Dejun, W. Baiqi, L. Shudan, X. Baifu, F. Honggang, S. Jiazhong, Journal of Molecular Catalysis A: Chemical 244 (2006) 193.
[66] B. Sarma, B.K. Sarma, Applied Surface Science 410 (2017) 557.
[67] D.-S. Lee, Y.-W. Chen, Journal of the Taiwan Institute of Chemical Engineers 45 (2014) 705.
[68] C. Sahoo, A.K. Gupta, Journal of Environmental Science and Health, Part A 50 (2015) 1333.
[69] V. Vaiano, O. Sacco, M. Stoller, A. Chianese, P. Ciambelli, D. Sannino, International Journal of Chemical Reactor Engineering 12(1) (2014) 1.
[70] K. Davididou, C. McRitchie, M. Antonopoulou, I. Konstantinou, E. Chatzisymeon, Journal of Chemical Technology & Biotechnology 93 (2018) 269.
[71] N.D. Cvjeticanin, N.A. Petranovic, Zeolites 14 (1994) 35.
[72] L.B. Reutergådh, M. Iangphasuk, Chemosphere 35 (1997) 585.
[73] V. Vaiano, M. Matarangolo, O. Sacco, D. Sannino, Applied Catalysis B: Environmental 209 (2017) 621.
[74] U.G. Akpan, B.H. Hameed, Journal of Hazardous Materials 170 (2009) 520.
[75] C. Zhu, L. Wang, L. Kong, X. Yang, L. Wang, S. Zheng, F. Chen, M. Feng, Z. Huang, Chemosphere 41 (2000) 303.

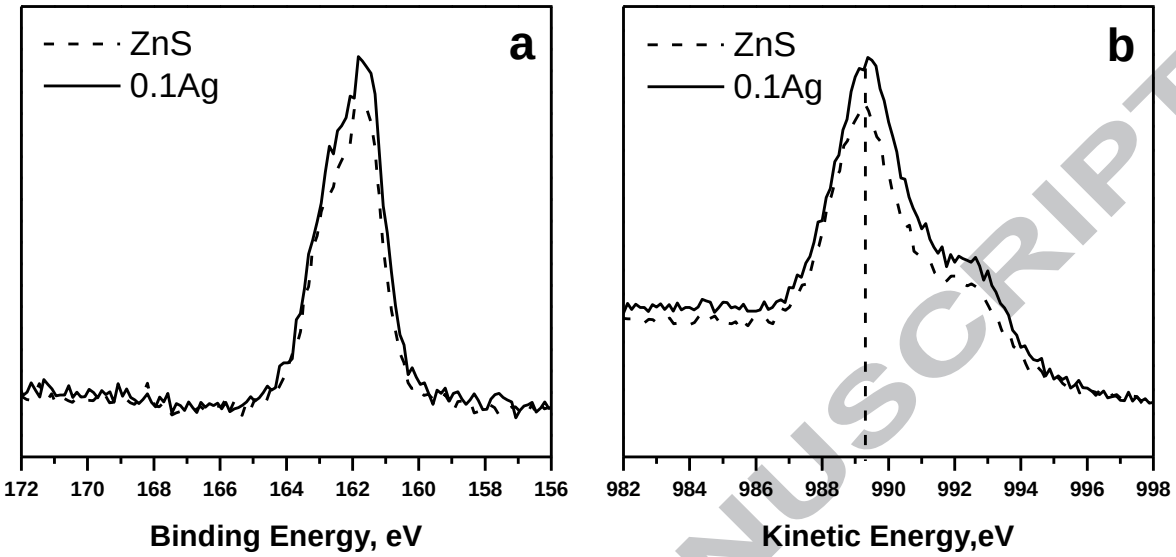

Figure 1 (a) S2p and (b) ZnLMM spectra relevant to bare ZnS (dashed curves) and to 0.1Ag sample (solid curves)

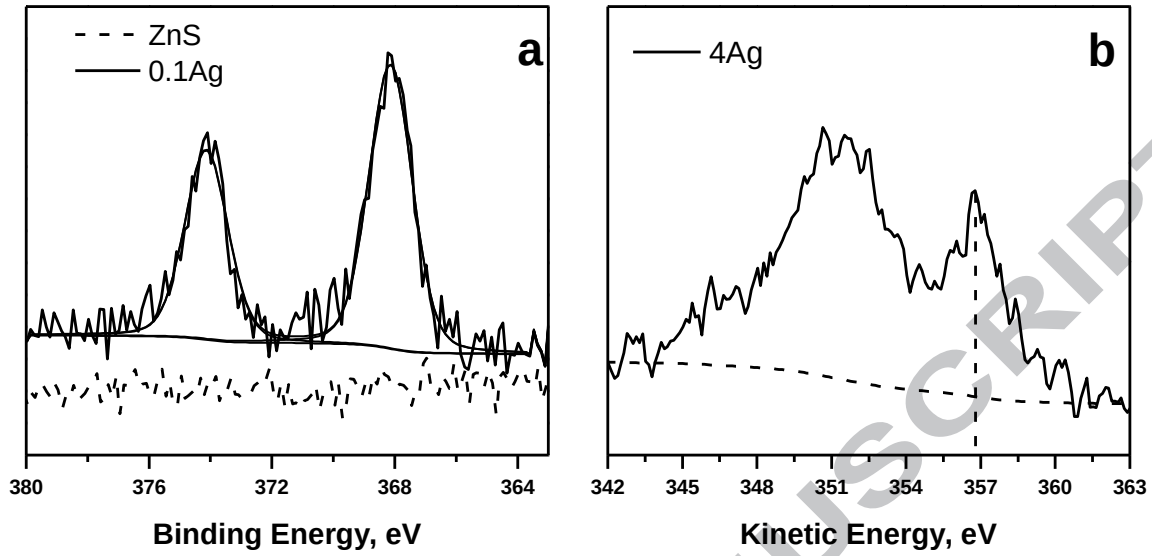

Figure 2 (a) Ag3d spectra relevant to bare ZnS (dashed curves) and to 0.1Ag (solid curves). Curve-fit of Ag3d doublet is shown; (b) AgMNN region associated to 4Ag. Auger peak position is indicated by the vertical dotted line.

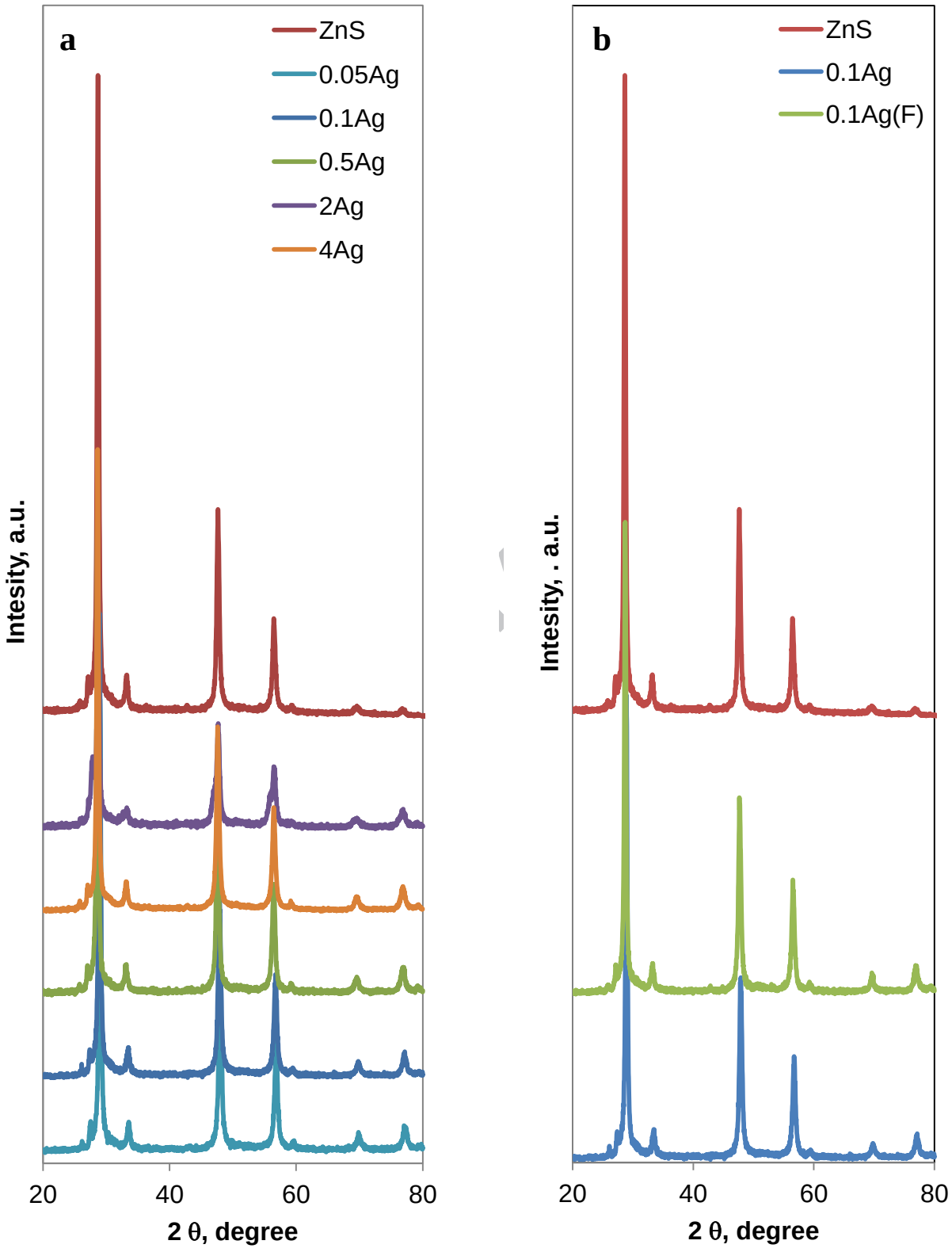

Figure 3 XRD patters of (a) ZnS and Ag/ZnS samples and (b) ZnS, 0.1Ag and 0.1Ag(F)

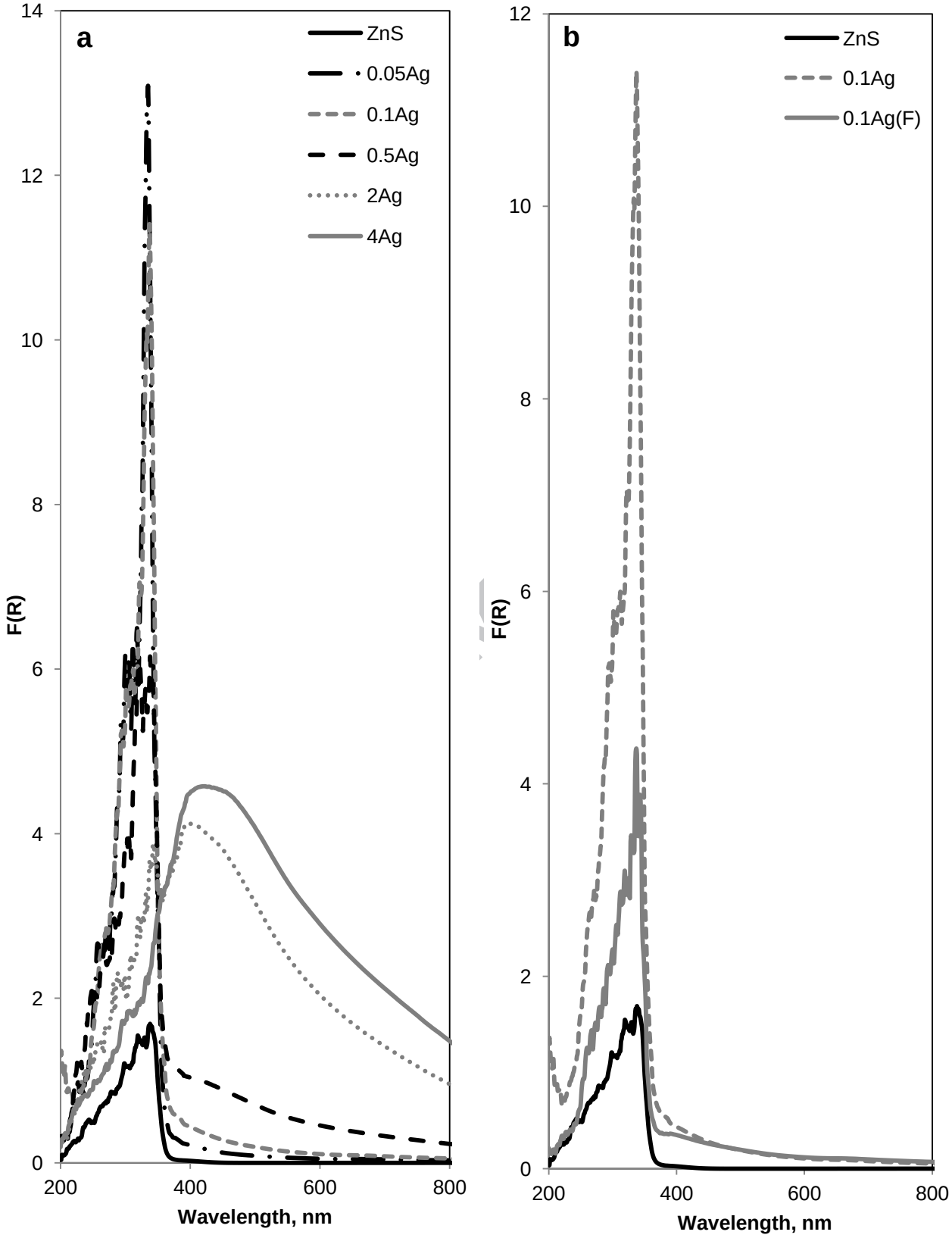

Figure 4 Kubelka Munk from UV-Vis spectra in the range 200-800nm for (a) bare ZnS and Ag/ZnS samples; (b) bare ZnS, 0.1Ag and 0.1Ag(F) samples

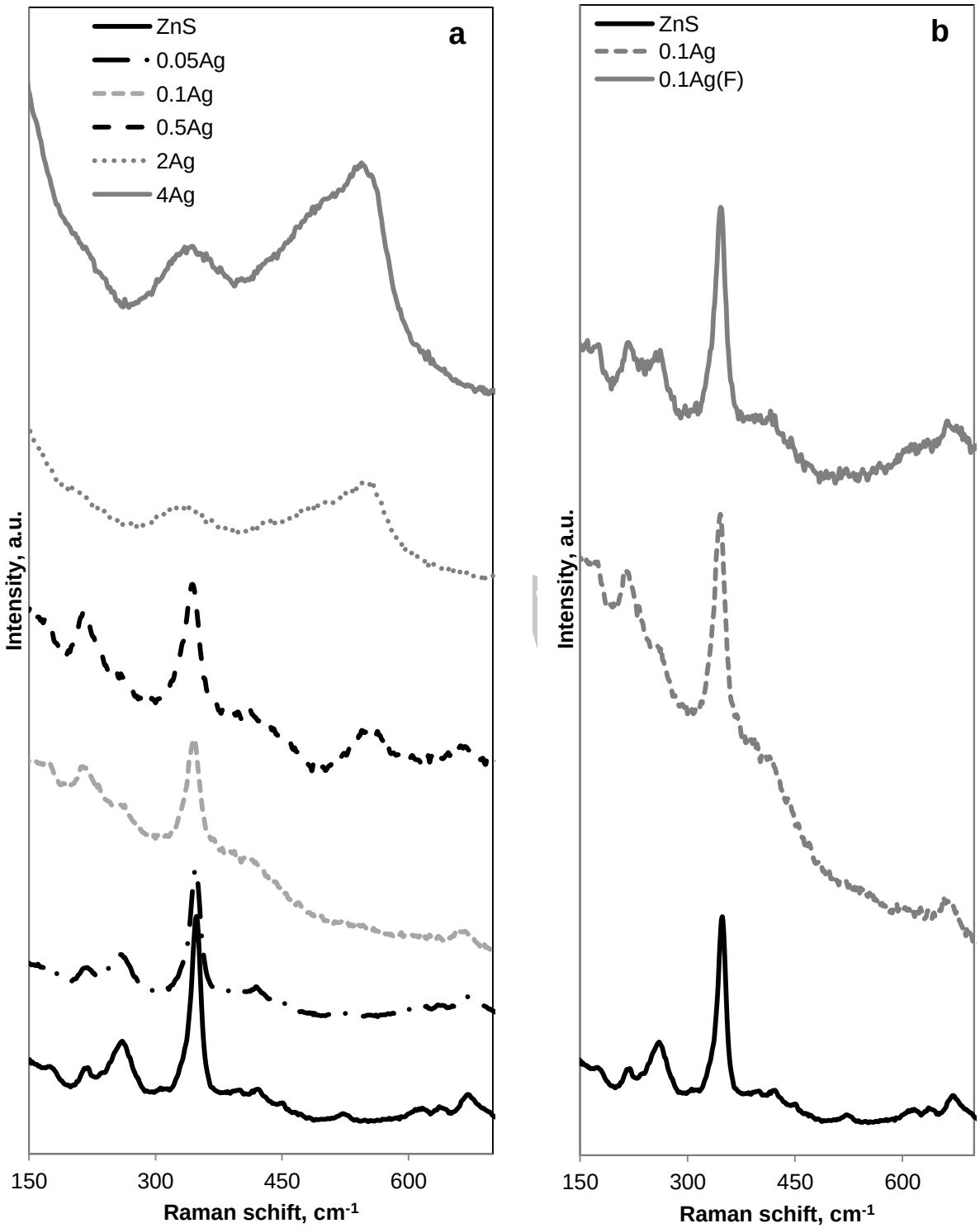

Figure 5 Raman spectra of (a) bare ZnS and Ag/ZnS samples and (b) bare ZnS, 0.1Ag, 0.1Ag(F)

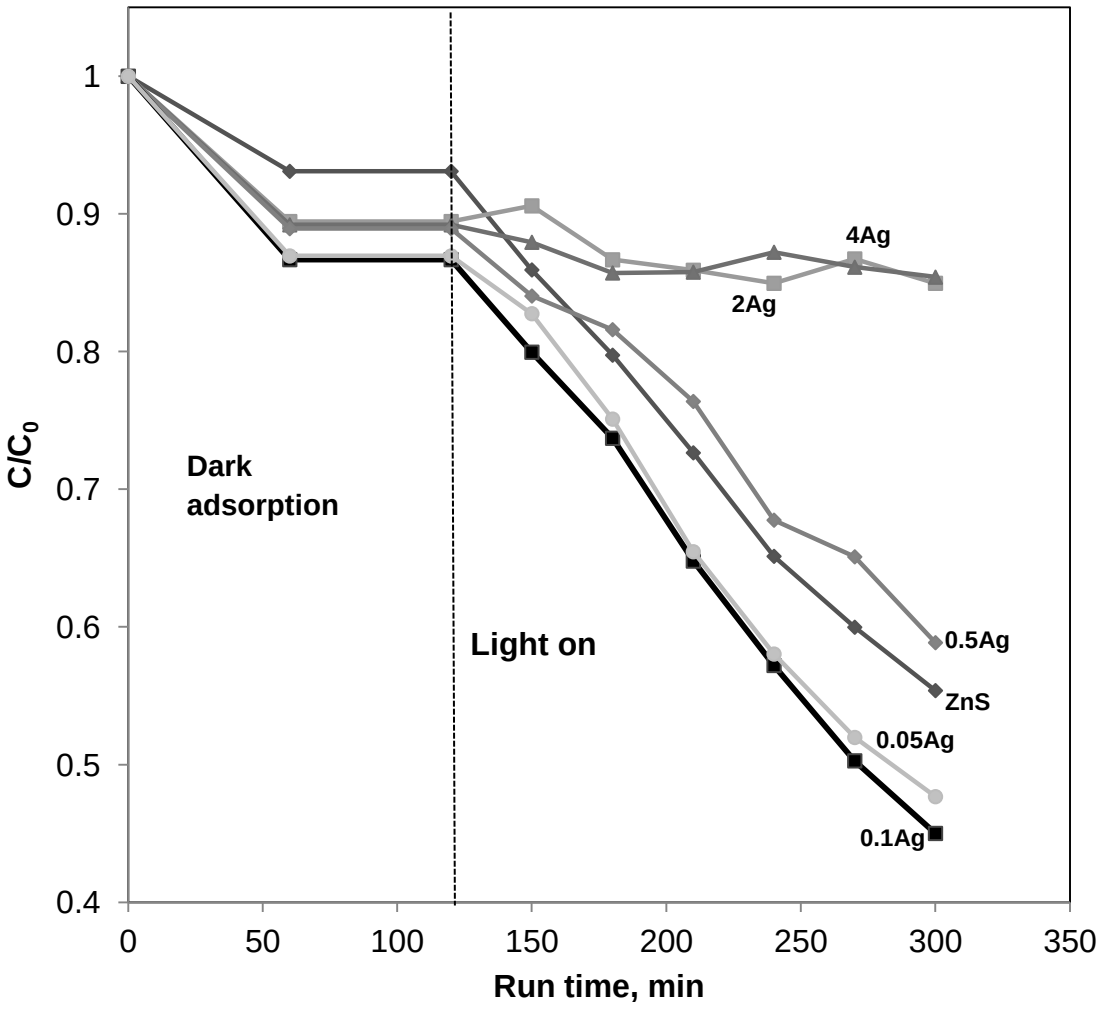

Figure 6 Photocatalytic MB decolourization over bare ZnS and Ag/ZnS catalysts; MB initial concentration: 15 mg L^{-1}; solution volume: 100 ml; photocatalyst dosage: 3g L^{-1}; light sources: UV lamps

Figure 7

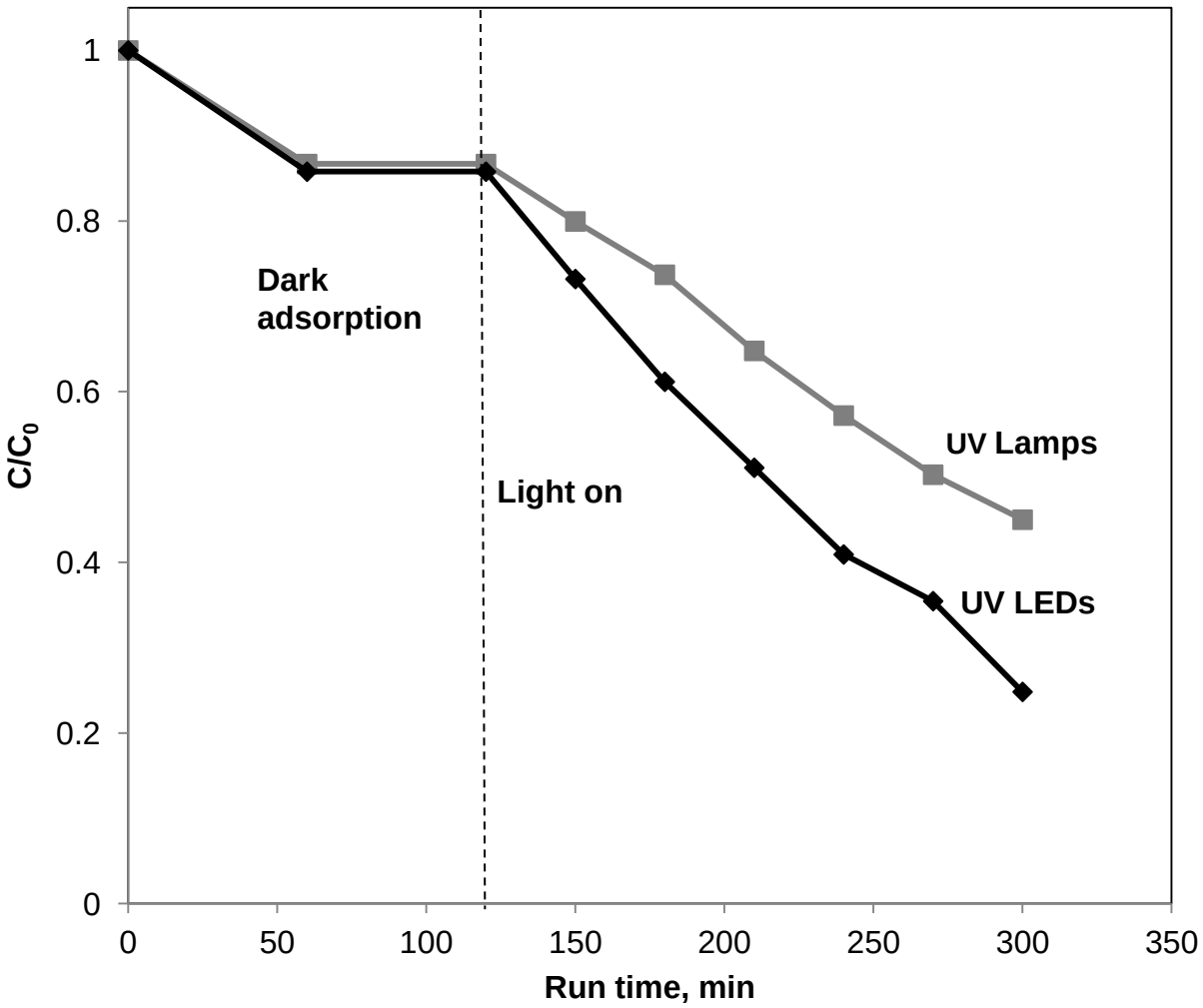

Figure 7 Photocatalytic decolourization of MB in the presence of UV-LEDs and UV-lamps 0.1Ag photocatalyst; MB initial concentration: 15 mg L^{-1}; solution volume: 100 ml; photocatalyst dosage: 3 g L^{-1}

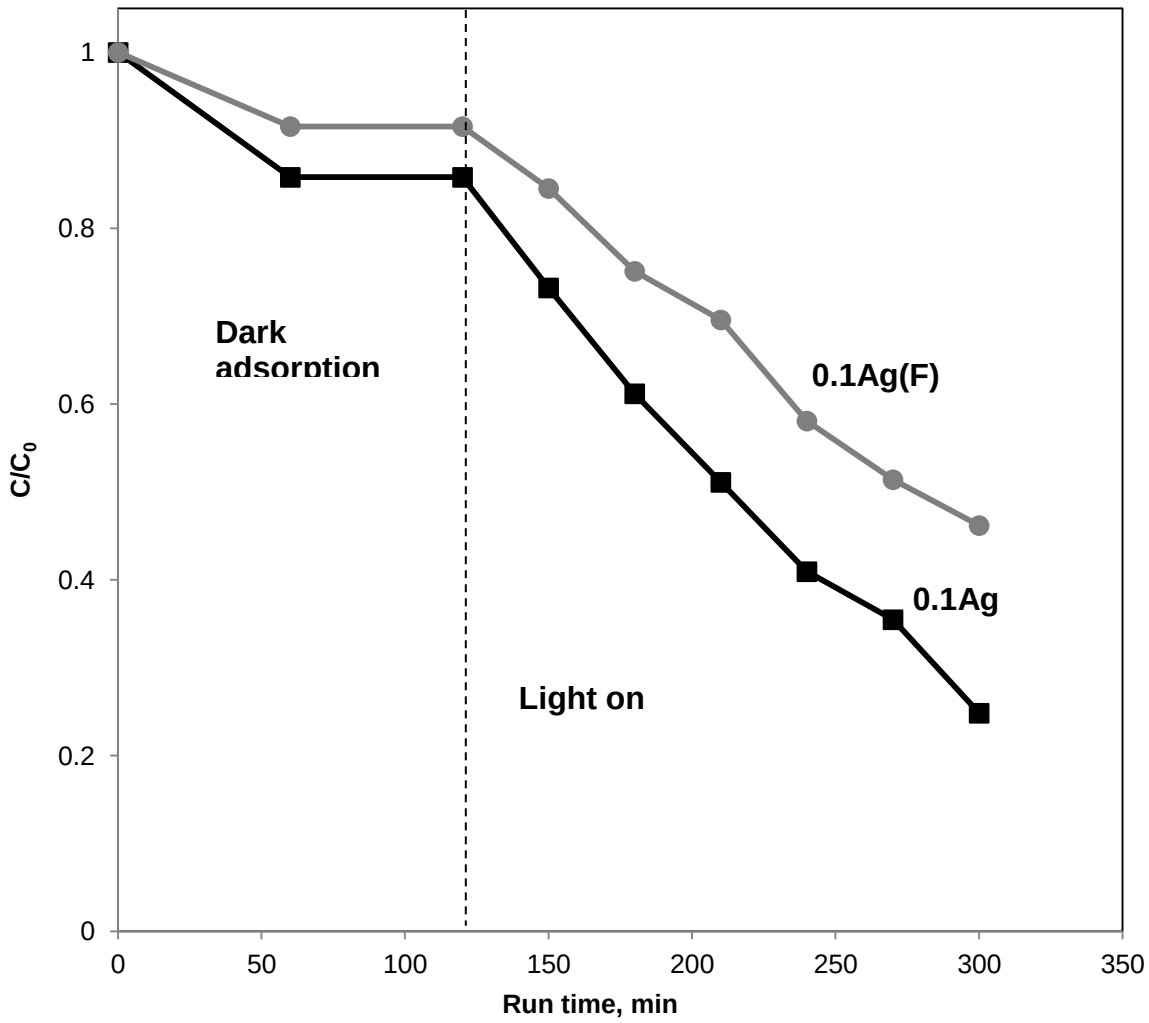

Figure 8 Photocatalytic MB decolourization under UV light (LEDs) over 0.1Ag and 0.1Ag(F) catalysts; MB initial concentration: 15 mg L^{-1}; solution volume: 100 ml; photocatalyst dosage: 0.3g L^{-1}

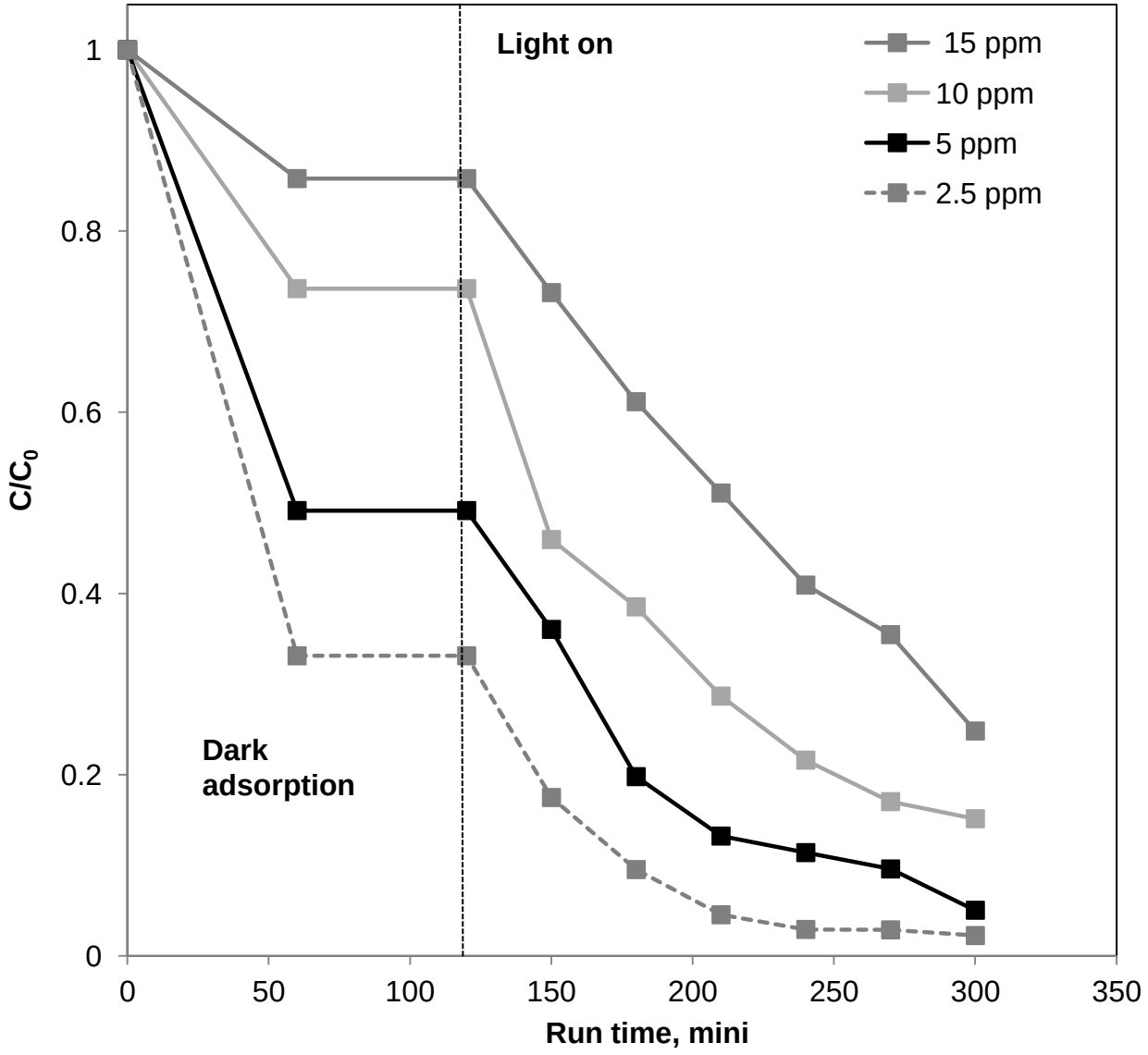

Figure 9 Influences of MB initial concentration; photocatalyst: 0.1Ag; solution volume: 100 ml; photocatalyst dosage: 0.3g L^{-1}; light sources: UV LEDs

Figure 10

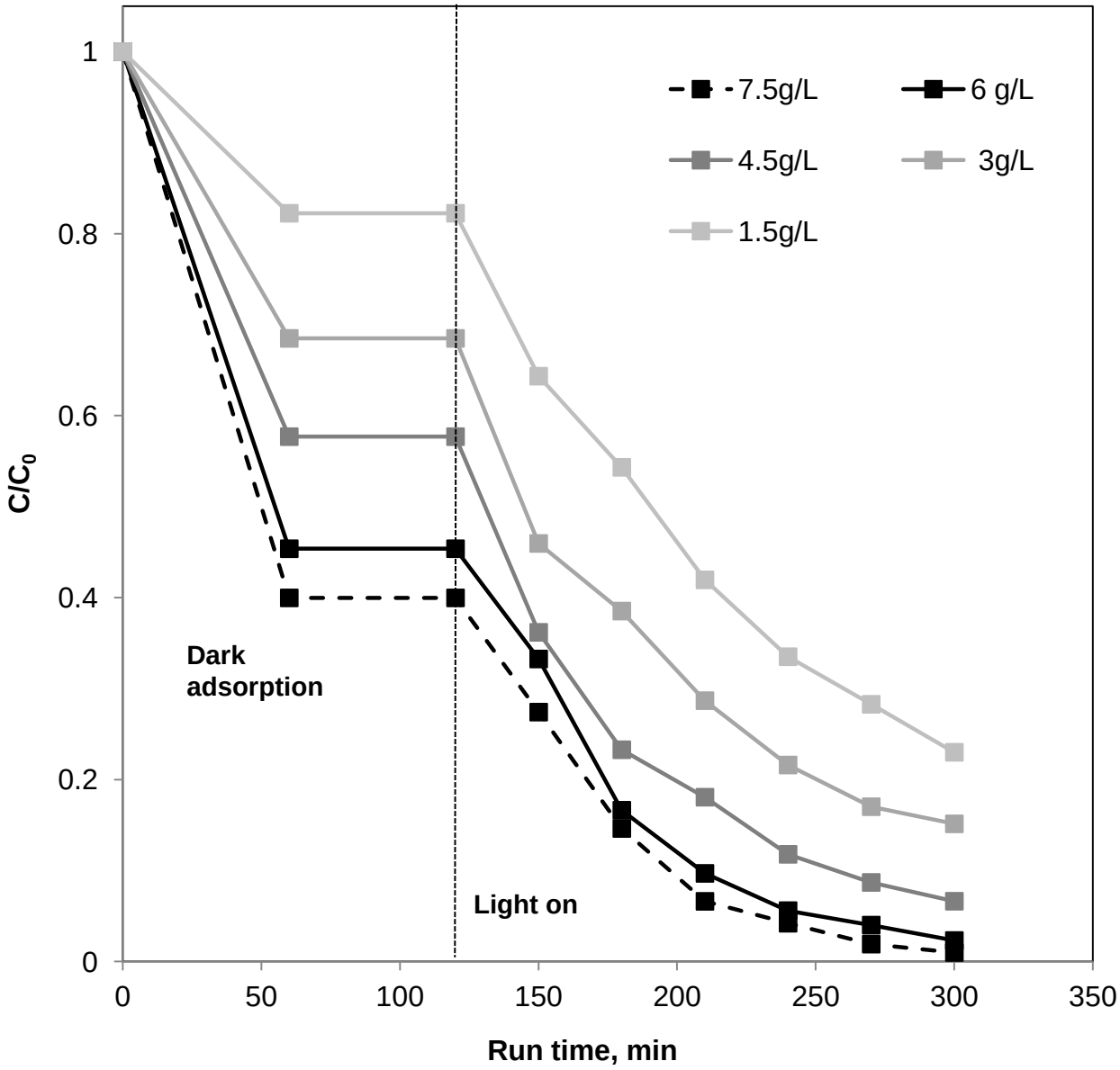

Figure : Influences of photocatalyst (0.1Ag) amount; initial concentration: 15 mg L^{-1}; solution volume: 100 ml; light sources: UV LEDs

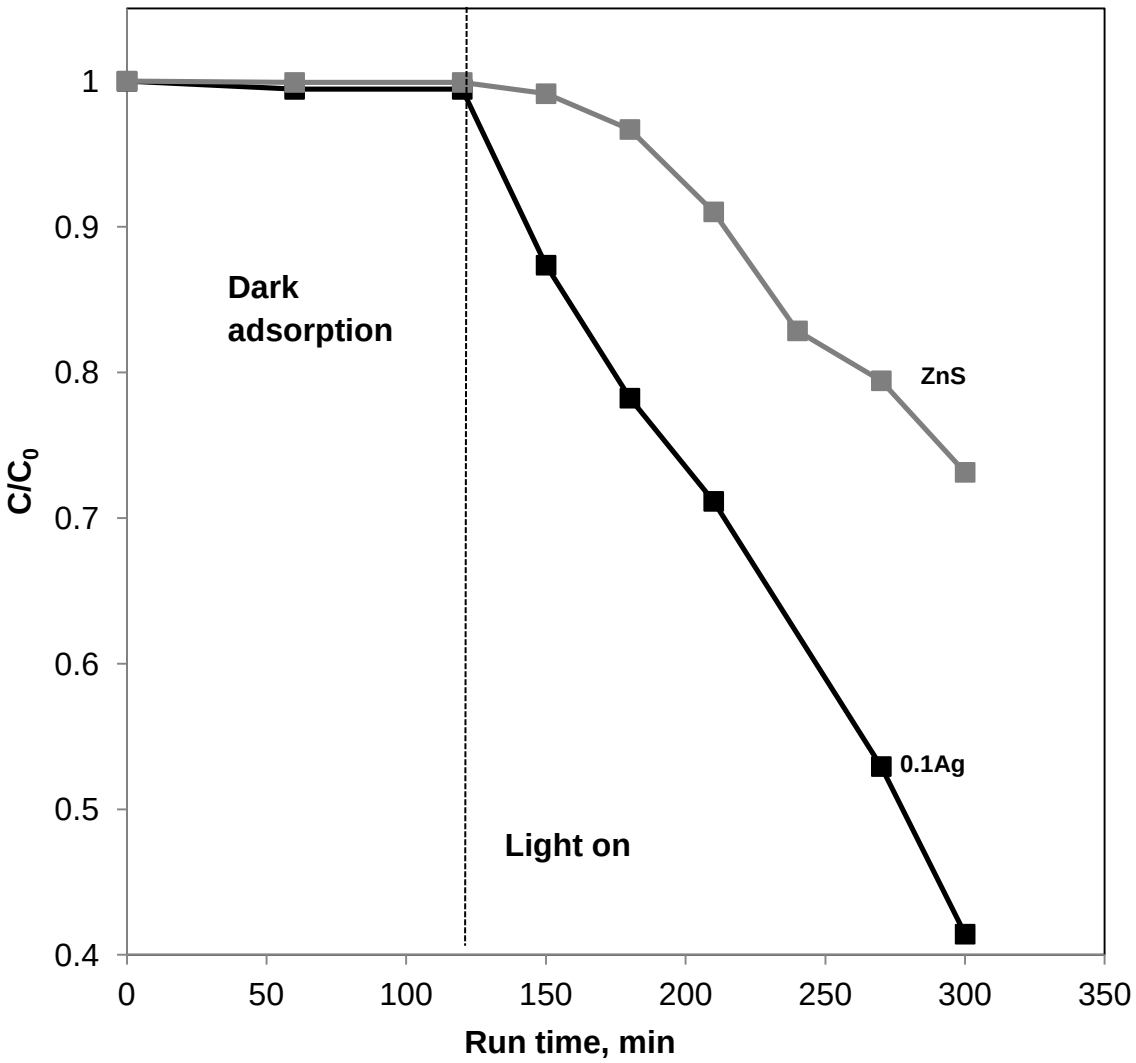

Figure 11 Photocatalytic degradation of phenol over bare ZnS and 0.1Ag catalysts; phenol initial concentration: 25 mg L^{-1}; solution volume: 100 ml; photocatalyst dosage: 0.3g L^{-1}; light sources: UV LEDs

Table 1 Ag nominal loading, crystallites size, specific surface area (SSA), band- gap energy (E_{bg}), valence band edge potential (E_{VB}) and conduction band CB edge potential (E_{CB})

Catalyst	**Nominal loading Ag, wt%**	**Crystallite size, nm**	**SSA, m^2/g**	**E_{bg}, eV**	**E_{VB}, eV**	**E_{CB}, eV**
ZnS	-	22	17	3.5	3.075	-1.555
0.05Ag	0.05	23	16	3.4	2.51	-0.99
0.1Ag	0.1	23	16	3.3	2.46	-0.94
0.1Ag (F)	0.1	22	17	3.4	2.41	-0.89
0.5Ag	0.5	24	15	2.8	2.46	-0.94
2Ag	2	25	14	2.1	2.16	-0.64
4Ag	4	26	13	1.8	1.81	-0.29

Table 2 Surface chemical composition of bare ZnS and Ag/ZnS for different Ag wt% loadings (error on atomic percentages (At%) is ±0.2% for Ag and Zn, and ±0.5% for the other elements). The surface silver weight % calculated from XPS data (Ag wt %) is reported in the last column.

Sample	**Zn%**	**S%**	**Ag%**	**C%**	**O%**	**Ag wt %**
ZnS	16.6	17.8	-	54.4	11.2	-
0.05Ag	30.3	28.9	0.6	29.0	11.2	1.8
0.1Ag	32.0	31.1	1.4	26.3	9.2	4.1
0.1Ag(F)	32.8	31.0	1.3	26.0	8.9	3.8
0.5Ag	31.6	30.1	1.3	27.3	10.5	3.8
2Ag	21.8	21.9	2.4	43.4	10.5	8.4
4Ag	22.9	21.1	5.7	37.3	13.0	17.8